

Scaling Structure Aware Virtual Screening to Billions of Molecules with SPRINT

Andrew T. McNutt^{1†}, Abhinav K. Adduri^{2†}, Caleb N. Ellington²,
Monica T. Dayao², Eric P. Xing^{2,3,4}, Hosein Mohimani²,
David R. Koes^{1*}

¹Computational and Systems Biology, University of Pittsburgh,
Pittsburgh, PA, USA.

²Computational Biology, Carnegie Mellon University, Pittsburgh, PA,
USA.

³Mohamed Bin Zayed University of Artificial Intelligence, Masdar City,
Abu Dhabi.

⁴Petuum Inc., Pittsburgh, PA.

*Corresponding author(s). E-mail(s): dkoes@pitt.edu;

†These authors contributed equally to this work.

Abstract

Virtual screening of small molecules against protein targets can accelerate drug discovery and development by predicting drug-target interactions (DTIs). However, structure-based methods like molecular docking are too slow to allow for broad proteome-scale screens, limiting their application in screening for off-target effects or new molecular mechanisms. Recently, vector-based methods using protein language models (PLMs) have emerged as a complementary approach that bypasses explicit 3D structure modeling. Here, we develop SPRINT, a vector-based approach for screening entire chemical libraries against whole proteomes for DTIs and novel mechanisms of action. SPRINT improves on prior work by using a self-attention based architecture and structure-aware PLMs to learn a co-embedding space for drugs and targets, enabling efficient binder prediction, search, and retrieval. SPRINT achieves SOTA enrichment factors in virtual screening on LIT-PCBA, DTI classification benchmarks, and binding affinity prediction benchmarks, while providing interpretability in the form of residue-level attention maps. In addition to being both accurate and interpretable, SPRINT is ultra-fast: querying the whole human proteome against the ENAMINE Real Database (6.7B drugs) for the 100 most likely binders per protein takes 16 minutes. SPRINT promises to enable virtual screening at an unprecedented scale,

opening up new opportunities for *in silico* drug repurposing and development. SPRINT is available on the web as *ColabScreen*: <https://bit.ly/colab-screen>.

Keywords: virtual screening, structure-based drug discovery, protein language models

1 Introduction

Virtual screening has emerged as a powerful tool for predicting drug-target interactions (DTIs) and guiding experimental efforts, but conventional structure-based methods like molecular docking are often too slow for proteome-scale analyses [1]. This limitation hinders their application in crucial parts of the drug discovery process such as off-target prediction [2]. The need for scalable and interpretable virtual screening methods is particularly evident in, for example, antimicrobial drug discovery. The rapid emergence of antimicrobial-resistant pathogens poses a severe threat to public health [3], necessitating the development of new antibiotics with novel mechanisms of action to combat cross-resistances [4]. Effective antimicrobial virtual screening requires methods that are not only fast and scalable but also interpretable, enabling researchers to: 1) identify new drug candidates with on-target effects across thousands of microbial proteomes and minimal off-target effects in humans and 2) provide interpretations for predicted DTIs and potential mechanisms of action.

Recently, vector-based virtual screening has been proposed as an alternative to structure-based screening to efficiently predict DTIs, leveraging vector featurizations for molecules [5] and sequence models for protein targets [6–8]. One method, ConPLex [2], proposes co-embedding molecules and proteins into a shared vector space, where the distance between entities is proportional to interaction likelihood. This effectively reduces the task of computing a DTI to a dot product in the co-embedding space, enabling the screening of millions of molecules against the entire human proteome in 24 hours. However, ConPLex does not scale favorably when identifying DTIs across thousands of bacterial and fungal proteomes, and it cannot provide explanations of its DTI predictions. Similarly, DrugCLIP [9, 10] aligns the embeddings of protein pocket structures and ligands with contrastive learning such that similarity encodes the probability of interaction. They demonstrate state-of-the-art (SOTA) results on virtual screening benchmarks with a fraction of the compute time needed for other structure-based virtual screening methods. Their approach is restricted to structures for which binding pockets can be predicted using pocket detection algorithms or homology-based approaches; however, [11] estimated that almost half of all structured domains may lack obvious pockets in their experimental structures.

In this work, we propose SPRINT (Structure-aware PRotein ligand INTeraction) for fast and accurate vector-based DTI predictions. SPRINT implicitly uses structure information by featurizing proteins with SaProt [8], a transformer model trained by augmenting the standard amino acid vocabulary with discrete structure-tokens [12]. Instead of averaging the per-residue embeddings from SaProt, SPRINT uses a multi-head attention pooling scheme to learn a sequence-dependent aggregation for protein representation.

Table 1 AUPR on test sets for DTI prediction with co-embedding models across benchmarks (mean \pm std). Train, validation, and test splits for BIOSNAP, Unseen Drugs, Unseen Targets, BindingDB, and DAVIS are taken from [2]. The MERGED dataset is split by homology (see Appendix C for more details). * indicates that we did not do contrastive training on DUD-E with the ConPLex model.

Model	ConPLex	ConPLex-attn*	SPRINT-sm (10M)	SPRINT (16M)
Backbone	ProtBert	ProtBert	SaProt	SaProt
Pooling	Avg	Attn	Attn	Attn
BIOSNAP	0.883 \pm 0.004	0.904 \pm 0.005	0.936 \pm 0.001	0.858 \pm 0.001
Unseen Drugs	0.874 \pm 0.002	0.905 \pm 0.002	0.906 \pm 0.001	0.851 \pm 0.002
Unseen Targets	0.842 \pm 0.006	0.844 \pm 0.011	0.849 \pm 0.006	0.793 \pm 0.007
DAVIS	0.457 \pm 0.037	0.493 \pm 0.014	0.507 \pm 0.005	0.446 \pm 0.003
BindingDB	0.616 \pm 0.009	0.672 \pm 0.003	0.718 \pm 0.0004	0.588 \pm 0.0006
MERGED	0.414 \pm 0.004*	0.448 \pm 0.018	0.481 \pm 0.004	0.526 \pm 0.002

SPRINT is extremely fast: querying a single protein target against the ENAMINE REAL (6.7B drugs) database and predicting its top-100 binders takes 7ms when utilizing ChromaDB[13]. Our main contributions are summarized as:

- Achieving excellent performance on DTI classification (Table 1), virtual screening (Table 2), and binding affinity prediction (Table 3).
- Enhance the second place method in the second critical assessment of computational hit-finding experiments (CACHE) challenge.
- Enabling pan-proteome-scale DTI screens using vector store and retrieval, scaling to billions of molecules.
- Improving molecular property prediction using the molecule co-embeddings learned via predicting DTIs.
- Investigating attention weights and visualizing attention maps to interpret model predictions.

Our software is available on our GitHub repository: <https://github.com/abhinadduri/panspecies-dti> and is also available on the web as *ColabScreen*: <https://bit.ly/colab-screen>.

2 Results

2.1 Multi-head attention pooling improves DTI prediction

A limitation of the ConPLex framework is that it averages the per-residue embeddings obtained from PLMs [2]. As much of the relevant signal for DTIs is located in the binding pocket residues, average pooling can noise the contact map information carefully learned by PLMs through self-attention [14], particularly in the longer sequence-length regime. Retraining the ConPLex model with an attention-based, learned aggregation function [15] achieves SOTA predictive scores for DTIs on most benchmarks (Table 1), even when using the same ProtBert model [6].

Table 2 Virtual Screening results on LIT-PCBA. SPRINT-ProtBert replaces SaProt with the ProtBert model, and SPRINT-Average replaces learned aggregation with average pooling and additional MLP layers. Parameter counts are shown in parentheses.

	AUROC (%)	BEDROC (%)	EF		
			0.5%	1%	5%
Surflex [20]	51.47	-	-	2.50	-
Glide-SP [21]	53.15	4.00	3.17	3.41	2.01
Planet [22]	57.31	-	4.64	3.87	2.43
GNINA [23]	60.93	5.40	-	4.63	-
DeepDTA [24]	56.27	2.53	-	1.47	-
BigBind [25]	60.80	-	-	3.82	-
DrugCLIP [9]	57.17	6.23	8.56	5.51	2.27
SPRINT-Average (15.7M)	67.49	7.80	7.23	6.26	3.71
SPRINT-ProtBert (15.9M)	73.4	11.9	11.68	10.19	5.27
SPRINT (16M)	73.4	12.3	15.90	10.78	5.29

To see how the learned aggregation scales with the available training data, we trained a SPRINT model on a huge dataset of DTIs, which we refer to as “MERGED”, [16] combining DTI data from PubChem [17], BindingDB [18], and ChEMBL [19] (further details can be found in Appendix C). Our largest model, SPRINT, uses 3-layer MLPs to encode molecules and proteins after multi-head attention pooling, in contrast to SPRINT-sm’s single-layer MLPs. SPRINT exhibits overfitting on the BIOSNAP, BindingDB, and DAVIS datasets but significantly improves performance on the much larger MERGED dataset (Table 1), confirming that there is value in scaling the SPRINT model size as we increase the amount of training data.

LIT-PCBA[26] is a challenging, commonly used virtual screening benchmark that addresses biases in the previously used DUD-E dataset [27] to explicitly enable validation of machine learning models. However, the activity labels in LIT-PCBA are derived from dose-response bioassays reported in PubChem [17], which may introduce noise and variability that could potentially impact the reliability of model evaluations. To evaluate the performance of SPRINT models at virtual screening on LIT-PCBA in the zero-shot setting, we pre-trained the deeper SPRINT (16M) model on the MERGED dataset after removing all protein sequences with $\geq 90\%$ sequence homology to the LIT-PCBA set using MMSeqs2 [28]. We see that the structure-aware SPRINT models significantly outperform competitor methods in AUROC, BEDROC ($\alpha = 0.85$), and across all enrichment factor thresholds (Table 2). The SPRINT models outperform similarly sized models trained using ProtBert featurizations and multi-head attention pooling (SPRINT-ProtBert), and models trained using SaProt featurizations and average pooling (SPRINT-Average) demonstrating the importance of structure and self-attention.

We further evaluate SPRINT for binding affinity prediction on the Therapeutic Data Commons (TDC) ‘BindingDB_Patent’ Leaderboard[29]. We see in Table 3 that SPRINT using both ProtBert, ESM2, and SaProt PLMs are competitive with the top-ranking model on the leaderboard, Otter-Knowledge-Ensemble[30]. This is notable, as the top ranking model is an ensemble of four knowledge graph-refined protein and ligand representations with each set of representations fine-tuned on a separate

Table 3 Pearson’s Correlation Coefficient on the TDC BindingDB.Patent Leaderboard (mean \pm std).

Model	Pearson’s Correlation Coefficient
Otter-Knowledge-Ensemble[30]	0.588 \pm 0.002
SPRINT-ProtBert	0.593 \pm 0.005
SPRINT-ESM2	0.582 \pm 0.012
SPRINT	0.588 \pm 0.011

dataset of protein-ligand interactions. All of the models start with ESM2 and Morgan fingerprint embeddings for the protein and ligand, respectively. We see that the SPRINT-ESM2 model performs similar to the Otter-Knowledge-Ensemble, an ensemble of refined ESM2 and Morgan representations. The SPRINT models match the performance while only observing the BindingDB.Patent training set. Interestingly, both ProtBert and ESM2 outperform SaProt in this task, despite SaProt performing better in previous tasks (Tables 1 and 2).

2.2 Enhancing Real-World Virtual Screening in CACHE2

The Critical Assessment of Computational Hit-Finding Experiments (CACHE) [31] serves as a benchmark for prospective evaluation of virtual screening methods through experimental validation of predicted hits. CACHE challenge 2 focused on the RNA binding site of SARS-CoV-2 NSP13, a helicase representing the most conserved site across coronaviruses [32] with no known inhibitors. . Crystal structures with bound fragments in the RNA-binding site exist, with PDB ID 5RLZ used for virtual screening. The second-place team [33] implemented a DeepDocking [34] approach using GNINA [1, 23]. They first filtered the Enamine REAL database for drug-like properties, reducing it to 4.4 billion molecules. Then, a random sample of 100,000 molecules (Batch 0) was docked against the 5RLZ structure using GNINA, and a surrogate model was trained to predict the docking score directly from a fingerprint of the molecule [5]. The entire database was scored with the surrogate model, and the top-scoring 100,000 molecules (Batch 1) were docked again with GNINA to produce training data for a new surrogate model. This process was repeated until the docking scores converged (Batch 5), as shown in Figure 1.

To evaluate the utility of SPRINT in filtering a compound database for high-likelihood binders and speeding up the DeepDocking process, we used SPRINT, pretrained on the MERGED dataset, to predict DTI scores for the filtered Enamine REAL database against the same virtual screening structure (5RLZ). We selected the highest-scoring 100,000 molecules from the filtered database and docked them using GNINA, following the same docking protocol as [33]. The virtual screening scores (CNN VS [1]) of our docked compounds are compared to the batches of GNINA DeepDocking in Figure 1. Molecules selected by SPRINT had a higher average CNN VS score (3.10) than Batch 0 of DeepDocking (2.59), and are more distributionally similar to Batches 1, 2, and 3. Notably, SPRINT finds 16 diverse, high-scoring molecules (CNN VS >

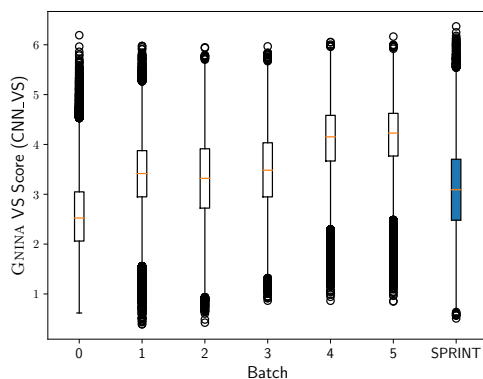


Fig. 1 GNINA CNN VS scores of the molecules found during DeepDocking and the molecules picked with SPRINT.

6) shown in Figure D2, while only 6 high-scoring molecules are found through DeepDocking (with one high-scoring molecule found during the initial random selection, Batch 0).

2.3 Structure-aware protein embeddings improve attention maps

Following training on the MERGED dataset with either ProtBert or SaProt as the PLM backbone for SPRINT, we analyze the attention patterns learned on a set of single-chain protein-ligand binding structures. We find that models with the greatest enrichment factors on LIT-PCBA, which are trained by sampling many negative DTIs for each positive DTI, have sparse attention that focuses on residues very distant from ligand interactions (Figures E3, F4, and F6). Therefore, we focus our attention analysis on SPRINT models trained with equal positive and negative sampling (LIT-PCBA results are provided in Table C2). All but one of the ProtBert attention heads attend less to the binding residues than they do to the non-binding residues (Figure 2). By introducing explicit knowledge of the protein’s structure with SaProt, we find more heads attending to the binding residues than the non-binding residues on average. We visualize the attention on the bound structure of a serine/threonine kinase (PDB ID: 2X4Z) in Figure 3 (additional visualizations provided in Appendix F). Both models have sparse attention maps, with only a handful of residues with non-trivial attention values per head. Attention head 2 of the SaProt model pulls out several residues near the binding site of the kinase, while none of the Protbert heads have much, if any, attention on the residues near the binding site, instead focusing on the edges of the protein.

Although the learned aggregation layer allows for model interpretation, we find there is little biological relevance for the attention patterns of the model at its current scale. For example, we compare the attention patterns to a multiple sequence alignment (MSA) of 497 human kinase domains from [35] and find that both models attend to non-conserved residues of the kinase that could identify the exact protein with a small residue fingerprint.

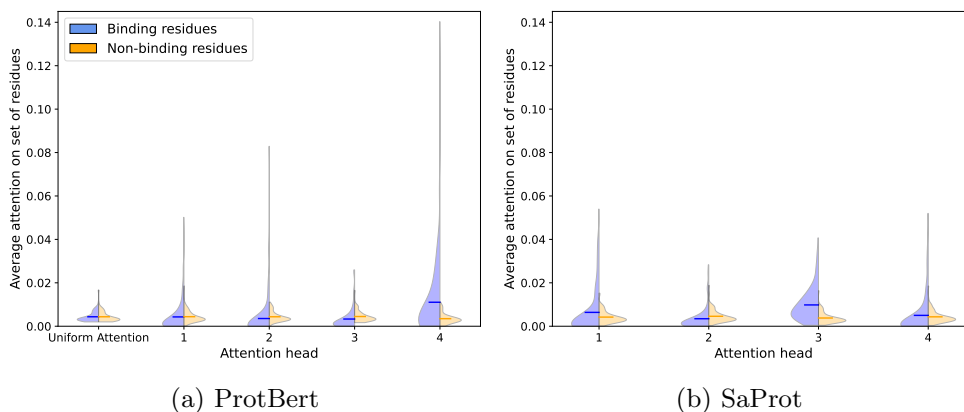


Fig. 2 Comparing the average attention weight of binding and non-binding residues on our set of 109 single-chain protein-ligand binding structures after training on the MERGED Dataset (Methodology detailed in Appendix E). We visualize the Protbert and SaProt models trained with equal positive and negative sampling. The horizontal line indicates the average across the proteins. Visualizations of the ProtBert and SaProt models trained with increased negative sampling are in Figure E3).

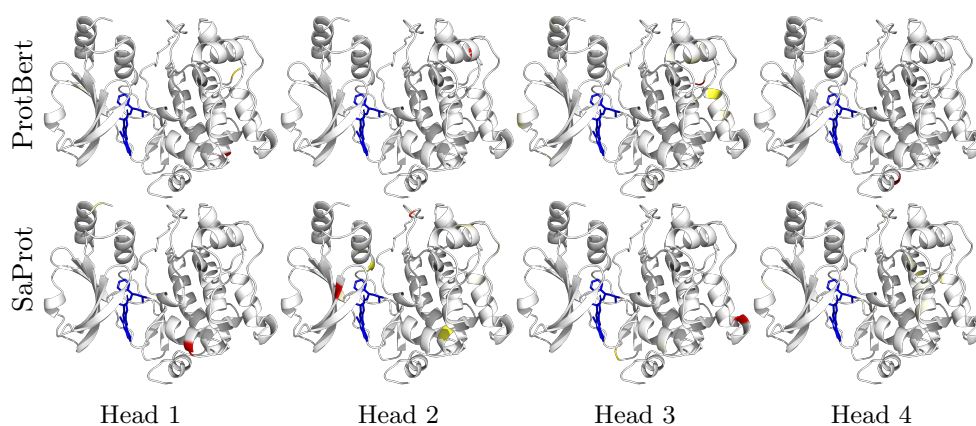


Fig. 3 Analyzing the attention on PDB ID 2X4Z using ProtBert and SaProt models trained with equal ratio of positive and negative examples (identical models trained with different initial random seeds visualized in Figures F5 and F7; models trained with increased negative sampling visualized in Figures F4 and F6). Each column is a different attention head. Gradient from white to red indicates the attention weight, where white is no attention and red is max attention for that head. The ligand is shown in blue.

2.4 SPRINT enables querying binding partners from 5132 proteomes

To demonstrate the utility of SPRINT at the pan-species-proteome scale, we constructed a dataset of 5,043 bacterial proteomes, 88 fungal proteomes, and the human proteome, containing 4,291,525 total protein sequences. To store and query the co-embeddings, we use the Chroma vector store[13], a tool developed for semantic search

and retrieval-augmented generation in natural language processing. The scaling properties of this framework are highly favorable (Fig. 4): querying a ligand for the 100 most likely binders against the entirety of UniProt (60M sequences) takes 0.0001s, and querying all 2e6 molecules in ChEMBL for each of their 10 most likely binders against the 4.3M proteins in our multi-species dataset takes less than 4 hours. As a proof of concept, we co-visualized several antimicrobials and drugs with their known protein targets across microbial proteomes (Fig. A1).

2.5 Pre-training to predict DTIs improves property prediction

To benchmark the usefulness of DTI co-embeddings for marginal property prediction, e.g., predicting the properties of a compound only from its molecular graph, we computed SPRINT DTI co-embeddings for several drug-like compounds [36] and natural products [37]. Concatenating the SPRINT-sm molecule co-embedding to a Morgan fingerprint consistently outperformed an equivalently sized neural network using only the Morgan fingerprint as input (Table B1). However, we observe that using only the SPRINT embedding in these tasks degrades performance, suggesting that SPRINT embeddings can synergistically enhance traditional fingerprints.

3 Methods

To enable fast and accurate screens, we seek a co-embedded representation of drugs and protein targets where a simple similarity metric indicates binding likelihood. Let D and T denote the random variables representing drugs and targets, f and g denote the choice of frozen drug and target encoders, and C_d and C_t denote modality-specific neural networks that project drug and target embeddings, respectively, into a shared co-embedding space. Let Y denote the random variable representing drug-target interaction, where $Y = 1$ denotes an interacting pair, and $Y = 0$ denotes a non-interacting pair. Denoting latent co-embeddings $Z_d = C_d(f(D))$ and $Z_t = C_t(g(T))$, our model is:

$$P(Y = 1|Z_d, Z_t) = \sigma \left(\alpha \frac{Z_d}{\|Z_d\|} \cdot \frac{Z_t}{\|Z_t\|} \right) \quad (1)$$

where σ denotes the sigmoid activation function, and α is a constant scaling factor chosen to saturate the range of the sigmoid function, as unscaled cosine similarity ranges from $(-1, 1)$. In our implementation, we choose $\alpha = 5$. Our goal through training is to learn C_d and C_t that minimize binary cross-entropy loss against ground truth binding and non-binding pairs.

In addition to classifying drug-target binding, SPRINT is capable of predicting binding affinity without changing learned portions of the model. By replacing the cosine similarity with a dot-product and removing the final sigmoid, we can leverage

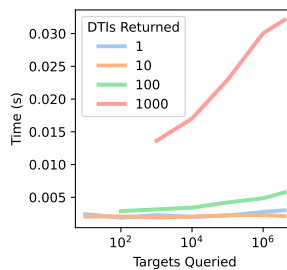


Fig. 4 Times for predicting the top DTIs for a ligand using vector search.

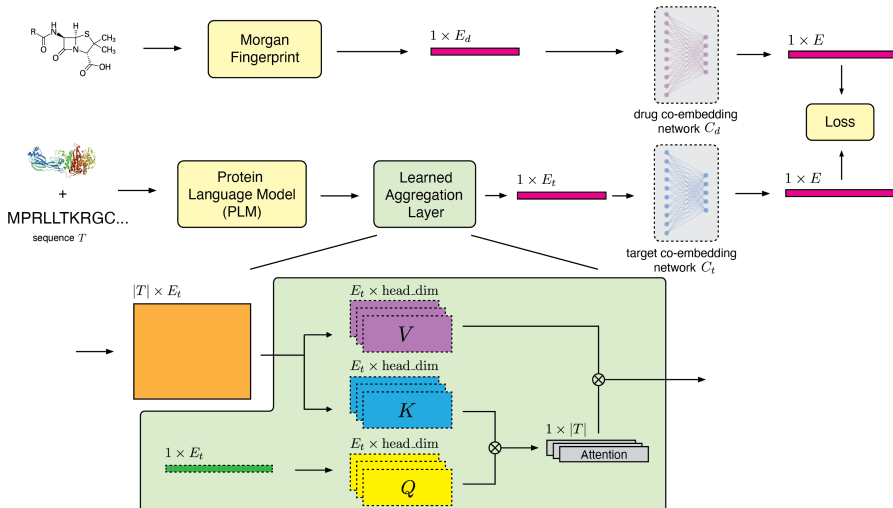


Fig. 5 SPRINT learns protein representations via a multi-head attention pooling scheme. Then, SPRINT learns a shared co-embedding space between molecules and protein targets via modality-specific neural networks C_d and C_t . The model is trained end-to-end via a binary cross entropy loss on binding and non-binding drug-target pairs, where the probability of interaction is computed as a sigmoid function of the cosine distance between the drug and target embeddings. The learnable parameters of the network are depicted with dashed borders.

SPRINT as a binding affinity predictor (Equation 2):

$$p\hat{K} = (Z_d \cdot Z_t) \quad (2)$$

where $p\hat{K}$ is the predicted $pK = -\log_{10}(K_d)$ to simplify training of the model on affinity values. Binding affinity regression models are trained to minimize mean square error loss against ground truth binding affinity by updating the weights of C_d and C_t .

For the drug encoder f , we use the Morgan fingerprint featurizer available in RDKit with bit length 2048 and radius 2 [5, 38]. For the target encoder g , we choose the structure-aware transformer model SaProt [8], a structure-aware protein language model that outputs per-residue embeddings, resulting in a $|T| \times E$ featurization for an input sequence T . SaProt optionally takes protein structure as an input to compute FoldSeek tokens for embedding [12]. We utilize AlphaFold2 [39] predicted structures to generate structure tokens when training the DTI model with SaProt. Unlike prior works, we employ multi-head attention pooling to aggregate these per-residue embeddings into a single vector representation of a protein (Fig. 5). This approach has two merits. First, we hypothesize that the model will be able to focus on information-rich residues due to the data-dependent nature of the attention scheme. Second, we can gain insights into the biological relevance of the attention patterns learned by the model by analyzing which residues are prioritized and how they may relate to known mechanisms of drug-target interaction. Further training details and hyperparameters are provided in Appendix C.

3.1 Data

We evaluate the performance of the SPRINT DTI prediction architecture on two tasks: interaction prediction and binding affinity prediction. SPRINT models trained for interaction prediction predict 1 if a drug and target pair interact and 0 otherwise. We utilize the same interaction prediction datasets as [2]: DAVIS, BIOSNAP, and BindingDB. DAVIS[40] and BindingDB[41] are both composed of drug-target paired with experimentally annotated dissociation constants, K_d . We utilize the same thresholds as [2] to set the binary labels: $K_d < 30$ are labeled as interacting and $K_d \geq 30$ are non-interacting. DAVIS consists of only 2086 interactions, BindingDB has 12668, and BIOSNAP has 19238 DTIs. The BIOSNAP[42] data originally consisted of only interacting drug-target pairs, so negative pairs are created by randomly sampling an equal number of drug-target pairs. The Unseen Drugs and Unseen Targets datasets are different splits of BIOSNAP from [43] to elucidate the zero-shot performance of DTI methods. The Unseen Targets dataset is constructed by randomly selecting 20% of the proteins from the full BIOSNAP dataset and assigning all interactions involving these proteins to the test set, while the remaining interactions are used for training. The Unseen Drugs dataset is constructed in an identical manner, but using the drugs rather than the targets.

All dataset splits are the same as [43], 70/10/20 for training, validation, and test, respectively. The training split is artificially subsampled to have an equal number of positive and negative interactions. To evaluate the scaling of the model on more training tokens, we utilize the “MERGED” dataset[16]. This dataset is composed of data from PubChem [17] (98.31%), BindingDB [18] (1.17%), and ChEMBL [19] (0.52%). We use the activity label of the dataset for our interaction label providing 929,656 positive pairs and 83,703,190 negative pairs. We split the data into train, validation, and test splits such that targets in train and validation have at most 90% sequence homology, and targets in train and test have at most 70% sequence homology (splits are further detailed in Appendix C).

We use the Therapeutic Data Commons (TDC)[29] BindingDB_Patent dataset for binding affinity prediction. Each drug-target interaction is labeled with an experimentally determined IC_{50} . The BindingDB_Patent dataset splits train and test with a temporal split on the patent date, everything before 2019 is included in the train and validation split, while everything 2019 and after is in the test set. Temporal splits are still prone to data leakage as new drugs are commonly developed for established protein targets as well as drugs being reused for new targets [44]. The TDC hosts a leaderboard for this dataset to continuously evaluate new methods on the same training and test splits. We reserve a random 20% of the training set as a validation set.

4 Discussion

Vector-based screens are extremely fast, enabling DTI prediction in regimes that would be impossible with structure-based approaches. We propose SPRINT, which improves on prior work using multi-head attention pooling that scales favorably as we increase the number of DTI training tokens. We show that SPRINT sets a new SOTA for DTI classification, virtual screening, and matches the performance of the top method on

Dataset	unique drugs	unique targets	positive interactions	negative interactions
DAVIS	68	379	1506	9597
BIOSNAP	4510	2181	13836	13647
BindingDB	10665	1413	9166	23435
MERGED	3529623	11958	929656	83703190
BindingDB_Patent	140746	477	N/A	N/A

Table 4 Statistics of DTI datasets

the TDC BindingDB_Patent leaderboard (Otter-Knowledge-Ensemble[30]) for binding affinity prediction, without the use of explicit knowledge graphs of protein-ligand interactions. We compare SPRINT using the ESM2 embeddings to their ensemble model using refined protein and ligand representations starting from the same representations as SPRINT. The SPRINT model achieves better binding affinity prediction than their four model ensemble which highlights the value of the attention pooling for the protein and the co-embedding space learned by the model. We demonstrate that SPRINT can perform virtual screening at pan-species proteome scales, e.g., for antimicrobial activities (Fig. A1). Lastly, we find that predicting DTIs via co-embedding is an effective pre-training strategy that enhances simple molecular property prediction (Table B1).

We also show that structure-aware PLMs like SaProt can confer performance gains in virtual screening. Interestingly, we find that the SPRINT models that perform best on the LIT-PCBA virtual screening benchmark, with increased negative sampling, have the least interpretable attention maps. We hypothesize that equal weighting of positive and negative drug-target pairs helps the model learn about residues that interact while increasing the amount of negatives dilutes the information of the positive examples. We compare the virtual screening performance of SPRINT on the second CACHE challenge to the second place computational method which utilizes DeepDocking. Notably, methods using DeepDocking have consistently placed in the top two for the three CACHE challenges in which final results are public, demonstrating its performance for finding hits from large libraries. SPRINT enables direct querying of the entire ENAMINE database, foregoing the initial random sample which can significantly bias the subsequent rounds of DeepDocking. After performing only 1/6th of the docking, SPRINT finds almost three times the number of high-scoring molecular scaffolds compared to GNINA DeepDocking. SPRINT’s top molecules can be a useful starting point for DeepDocking to ensure that chemical space is more effectively explored.

We envision the SPRINT framework and training task as a useful benchmarking tool for protein and molecule encoders. Future work will evaluate other structure-aware PLMs such as MULAN or S-PLM [45, 46], and other pre-trained molecule encoders like UniMol [47, 48], in the SPRINT framework for DTI prediction. Additional work to interpret the aggregated protein features through methods like InterPLM[49] could provide insight into the virtual screening predictions. We anticipate this technology will democratize virtual screening by enabling the discovery of lead molecules with a

fraction of the compute cost required by comparable, structure-based, virtual screening methods.

Supplementary information. Additional information provided in the appendices.

Acknowledgements. The authors would like to thank Ian Dunn for providing the filtered dataset used for the CACHE screen in addition to the results of their virtual screening method for comparison.

Please refer to Journal-level guidance for any specific requirements.

Declarations

Funding

A.M. and D.K. are supported by the R35GM140753 from the National Institutes of Health. A.A. and H.M. are supported by the United States Department of Agriculture, Agriculture Research Service (USDA-ARS) and by grants 5R01GM107550-10 and 1U24DK133658-01. C.E. and E.X. are supported by the R01GM140467 from the National Institutes of Health, and the 2040381 from the National Science Foundation. M.D. was supported by the F31LM014194 from the National Institutes of Health.

Competing interests

The authors declare no competing interests.

Data availability

DAVIS, BIOSNAP, BindingDB, and MERGED DTI classification datasets are available through our github: <https://github.com/abhinadduri/panspecies-dti>. The BindingDB DTI DG dataset for the TDC Leaderboard is available through the Therapeutics Data Commons: <https://tdcommons.ai/>. The Lit-PCBA evaluation benchmark is available through the original authors <https://drugdesign.unistra.fr/LIT-PCBA/>. The filtered Enamine REAL dataset used for the second CACHE challenge is too large for upload, but can be obtained from the authors upon reasonable request.

Code availability

All code to reproduce our results is available on our github repository: <https://github.com/abhinadduri/panspecies-dti>.

Author contribution

A.M.: conceptualization, methodology, writing-original draft, software, investigation, validation **A.A.:** conceptualization, methodology, writing-original draft, software, investigation, validation **C.E.:** conceptualization, methodology, software, writing-original draft **M.D.:** software, visualization, writing-review&editing **E.P.:** supervision, funding acquisition **H.M.:** supervision, funding acquisition **D.K.:** conceptualization, resources, supervision, funding acquisition, writing-review&editing

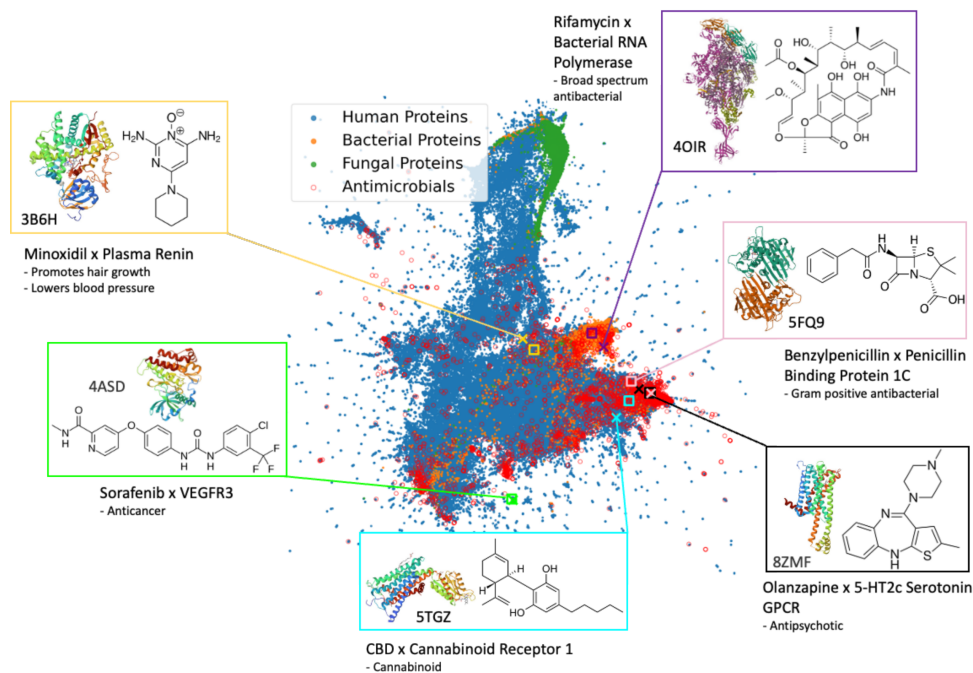


Fig. A1 UMAP visualization of the binding co-embedding space of drug-like small molecules and their protein targets across bacterial, fungal, and human proteomes. We see that antimicrobial compounds co-localize with regions of the shared latent space that contain human, bacterial, and fungal proteomes.

Appendix A SPRINT recovers known mechanisms of action

Our pan-species protein dataset is comprised of all predicted protein sequences in reference genomes from NCBI within the taxons bacteria, fungus, and human. Each taxon contained 3,379,854, 775,477, and 136,194 protein sequences respectively. We gathered a list of 3,112 natural products [37], as they are known to have a high prior likelihood for antimicrobial activity [50] and are out-of-distribution relative to our MERGED training dataset. We then co-visualized several antimicrobials and drugs with their known protein targets across microbial proteomes (Fig. A1), recovering several known mechanisms of action. The dataset is available to query at <https://bit.ly/colab-screen>.

Appendix B SPRINT co-embeddings improve property prediction

Current antimicrobial and toxicity screening approaches are often formulated as molecular property predictors, framing antimicrobial activity and toxicity to humans as inherent properties of drug molecules [36, 51–55]. Our results demonstrate that

Table B1 F1 scores for MLP classification models applied to molecule embedding strategies (mean \pm std). Models trained on Morgan fingerprints used a larger hidden size to match the size of models trained on fingerprints concatenated with embeddings.

Featurization	Antibacterial Task	Toxicity Task
Morgan Fingerprint	0.740 \pm 0.027	0.720 \pm 0.008
SPRINT-sm Embedding	0.687 \pm 0.012	0.656 \pm 0.015
Morgan Fingerprint + SPRINT-sm Embedding	0.749 \pm 0.016	0.735 \pm 0.006
SPRINT Embedding	0.614 \pm 0.027	0.631 \pm 0.023
Morgan Fingerprint + SPRINT Embedding	0.722 \pm 0.027	0.701 \pm 0.018

augmenting Morgan fingerprints with SPRINT-sm ligand embeddings consistently outperformed an equivalently sized neural network using Morgan fingerprints alone, when evaluated on both an antibacterial activity dataset [37] and a toxicity dataset [36] (Table B1). We hypothesize that vectorizing the DTI space allows property prediction methods to leverage information about target neighborhoods around a drug, enhancing performance and offering mechanistic explanations for these properties based on likely binding partners. The embeddings from the deeper SPRINT model consistently performed worse than those from the shallow SPRINT-sm model, suggesting that shallow transformations of the Morgan fingerprint work best in this setting. The standalone SPRINT embeddings achieved substantially lower performance than their concatenated counterparts, indicating that SPRINT embeddings may capture complementary molecular features to traditional fingerprints.

Appendix C Training details

DTI models are trained using the same train/val/test splits as [2] for the DAVIS, BindingDB, and BIOSNAP datasets. All structure tokens for SaProt were computed on AlphaFold2 [39] generated structures. Structures were downloaded from the AlphaFold Protein Structure Database if they existed. When no precomputed structure was available, ColabFold [56] was run with 2 random seeds to generate 10 energy minimized structures, and the minimized structure with the highest pLDDT was used. Structure tokens were generated with Foldseek[12], masking the structure token if the residue pLDDT was less than 70.

Specifically, the loss \mathcal{L} is written as

$$\mathcal{L} = \frac{1}{N} \sum_i^N \left[Y^i \log(\tilde{Y}^i) + (1 - Y^i) \log(1 - \tilde{Y}^i) \right] \quad (\text{C1})$$

$$\tilde{Y}^i = P(Y^i = 1 | Z_d^i, Z_t^i) = \sigma \left(\alpha \frac{Z_t^i}{\|Z_t^i\|} \cdot \frac{Z_d^i}{\|Z_d^i\|} \right) \quad (\text{C2})$$

Table C2 LIT-PCBA evaluation ablation of negative sampling. ‘1:1’ indicates equal sampling of positive and negative examples during training and ‘3:1’ indicates the preferred model training with 3 negatives sampled for every positive example.

Model	AUROC	BEDROC ($\alpha = 0.85$)	EF (0.5%)	EF (1%)	EF (5%)
SPRINT-ProtBert 1:1	71.53	7.78	6.81	5.87	3.86
SPRINT 1:1	72.71	10.16	10.31	8.86	4.73
SPRINT-ProtBert 3:1	73.4	11.9	11.68	10.19	5.27
SPRINT 3:1	73.4	12.3	15.90	10.78	5.29

where the protein, T^i , and drug, D^i , have been mapped to the SPRINT co-embedding space as Z_t^i and Z_d^i , respectively. $Y_i \in \{0, 1\}$ is a ground-truth label with value 1 if T^i and D^i are binders or 0 if they are non-binders. The pre-sigmoid scalar value, α , is used to expand the range of cosine-similarity to the domain of the sigmoid. We set α to 5. Models are trained for binary classification using standard, supervised cross-entropy loss.

Binding affinity regression models use the same architecture to learn the co-embedding space, but the final, non-learned components are removed. The sigmoid and pre-sigmoid scalar value are removed and the cosine similarity is replaced with a dot-product (Equation 2). This allows the magnitude of drug and target embeddings to impact the prediction as well as increasing the range to all real numbers. Regression models are trained with mean squared error loss.

ConPLex models are trained with the hyperparameters used in the original paper [2]. Our Attention Pooling models are trained with a learning rate of 1×10^{-5} and a dropout value of 0.05 for 250 epochs, keeping all other hyperparameters the same as ConPLex training. We set weight decay to 0.01 for the binding affinity regression model following hyperparameter tuning on the validation set. The model checkpoint with the highest validation AUPR for classification models and MSE for regression models during training is evaluated on the test set (Table 1 and 3).

To enable efficient training on the MERGED dataset, we featurize the unique proteins and molecules before training, storing their representations in memory-mapped files for quick retrieval using the Lightning Memory-Mapped Database Manager (LMDB) library. To address data imbalance in the binding data, for each epoch, we train using all of the drug-target binding pairs, and subsample an equivalent number of non-binding pairs without replacement. We observed that models trained with more negatives than positives (at a 3:1 ratio), achieved better virtual screening performance, but had less interpretable attention patterns (Tables 1, C2). Models are trained for 20 epochs. All other hyperparameters were kept the same.

The MERGED dataset splits were determined by clustering protein sequences using MMSegs2 [28] at 80% coverage threshold and 70% sequence identity, meaning two sequences appear in the same cluster if at least 80% of residues are aligned with at least 70% identity. Clusters were then assigned to splits by size, with smaller clusters preferentially assigned to test and validation sets until each contained approximately 10% of the total number of unique proteins. The remaining sequences were assigned to training. Drug-target interactions were then partitioned according to their protein

assignments. The final training, validation, and test sets contained 79.5%, 10.3%, and 10.2% of total interactions, respectively.

Appendix D High scoring molecules screened with SPRINT for NSP13 Helicase

We show the 2D depiction of the highest scoring molecules, according to GNINA's CNN VS, from SPRINT's screen of Enamine REAL in Figure D2. We see that the molecules represent diverse scaffolds.

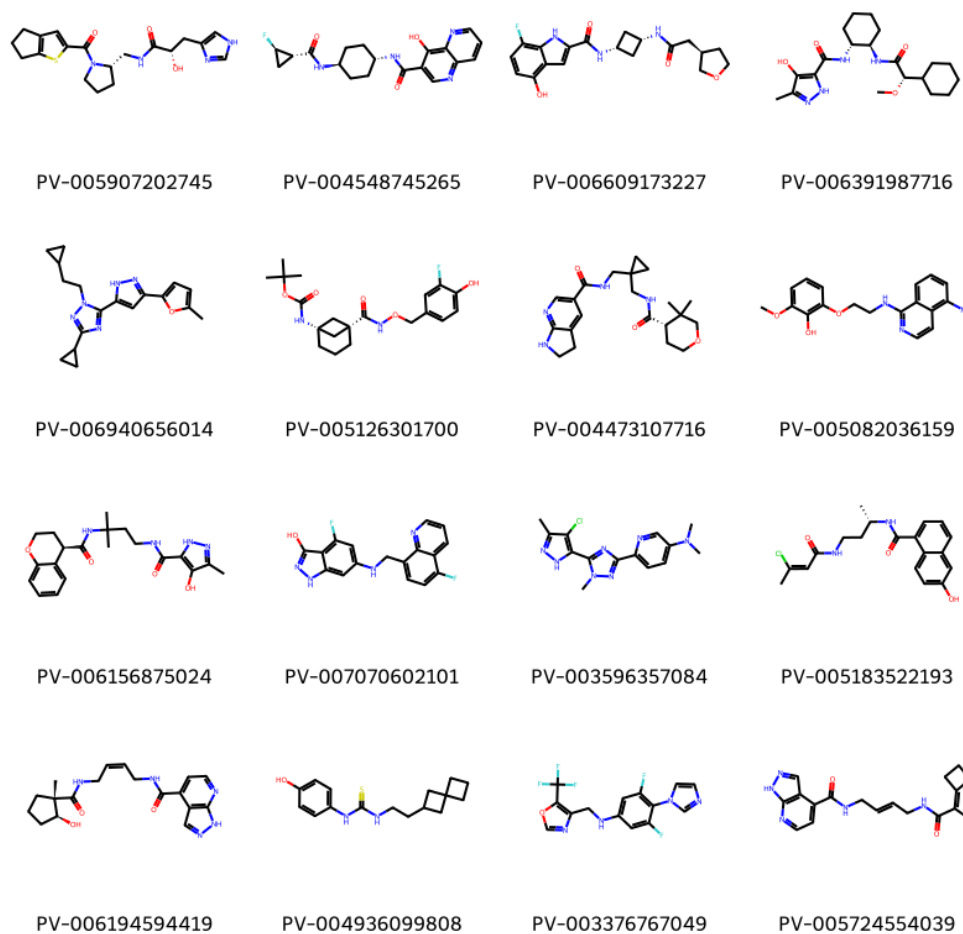


Fig. D2 2D depiction of the high-scoring (CNN VS > 6) molecules found by SPRINT for NSP13 Helicase.

Appendix E Investigating the learned aggregation layer

We investigate the attention pattern of our learned aggregation layer and compute the relative weighting of binding and non-binding residues. For this analysis, we use the intersection of the PDBbind refined v.2019 [57] dataset and the dataset created by [58]. The intersection of these datasets provides 109 single-chain, high-quality protein-ligand binding structures with annotated binding sites. Following the same protocol as [58], we determine binding residues based on a maximum heavy-atom distance of 5 Å between the residue and the ligand.

We first analyzed the attention patterns of each head in the learned aggregation layer to determine if any of the heads were selective for binding residues. We calculate the attention scores for each residue in the protein and compute the mean attention value for the binding residues and the non-binding residues. Figure 2 shows the average weight of the binding residues and non-binding residues across the dataset for the ProtBert and SaProt models trained with equal positive and negative sampling. We find the models trained with equal positive and negative sampling have more interpretable attention maps despite a decreased performance on the LIT-PCBA benchmark compared to models trained with more negative samplings. We compare the attention of all the models in Figure E3, visualizing three otherwise identical models trained with different initial random seeds. Interestingly, the PLM with the worst performance on the LIT-PCBA benchmark, ProtBert, shows the most attention to binding site residues relative to its attention to non-binding site residues. The structure-aware PLM, SaProt, has two seeds that attend to binding residues more than non-binding residues across most of the attention heads and one seed that pays very little attention to the binding residues. The SaProt seed that has the least attention for binding residues as compared to non-binding residues performs the best on the LIT-PCBA benchmark. Across all PLMs, there is a large variance in the attention to binding residues as the models initial random seed is changed.

We visualize the learned aggregation layers attention heads on the protein-ligand structures for both ProtBert and SaProt models in Figure 3 with additional visualizations provided in Appendix F and on our github.

Appendix F Structural visualizations

We visualize the attention patterns of the attention pooling layer on the protein-ligand bound structure of several PDB IDs. We compare the attention patterns of SPRINT models with ProtBert and SaProt trained on the MERGED dataset. We see across these diverse proteins and ligands that on average, the SaProt model attends to residues closer to the ligand, while the ProtBert models often attend to residues far from the binding site.

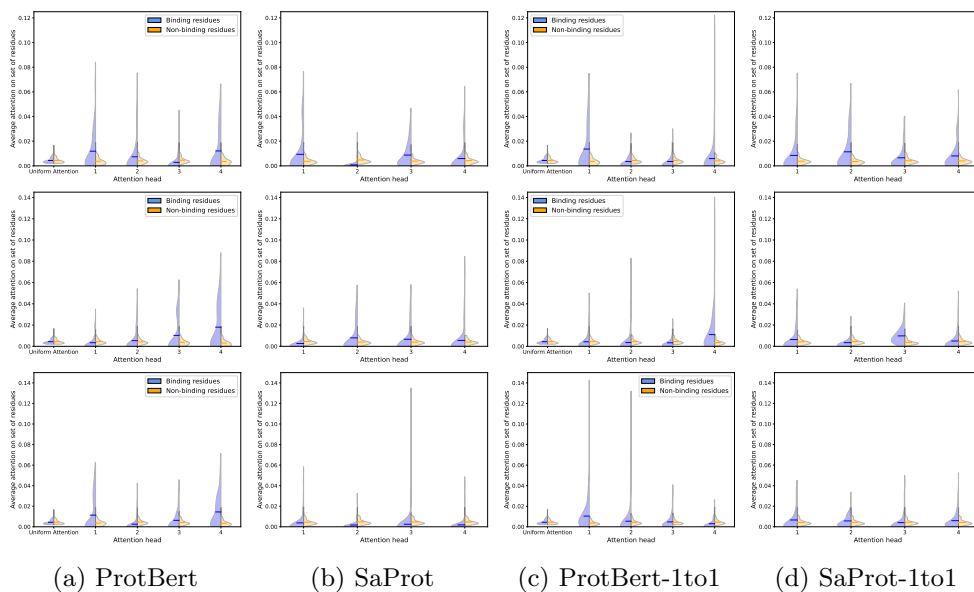


Fig. E3 Comparing the average attention weight of binding and non-binding residues on our set of 109 single-chain protein-ligand binding structures after training on the MERGED Dataset. The horizontal line indicates the average across the proteins. Each row is a different random seed and each column is a different PLM or different training regime, where ‘1to1’ indicates that a 1:1 positive to negative sampling ratio was used during training.

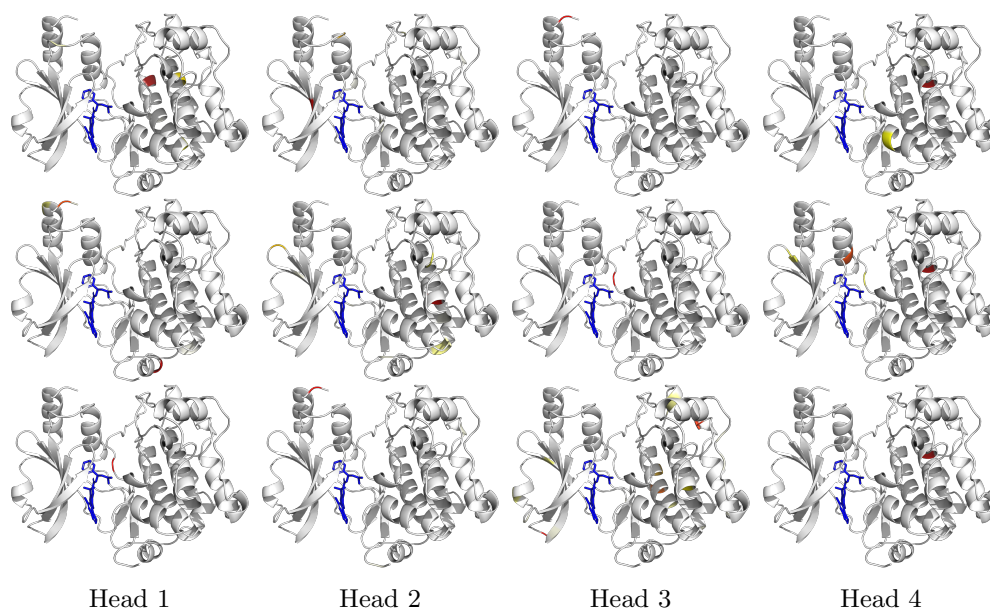


Fig. F4 Analyzing the attention of the ProtBert model on PDB ID 2X4Z. Each row is the ProtBert model trained with different seed. Each column is a different attention head. Gradient from white to red indicates the attention weight, where white is no attention and red is max attention for that head. The ligand is shown in blue.

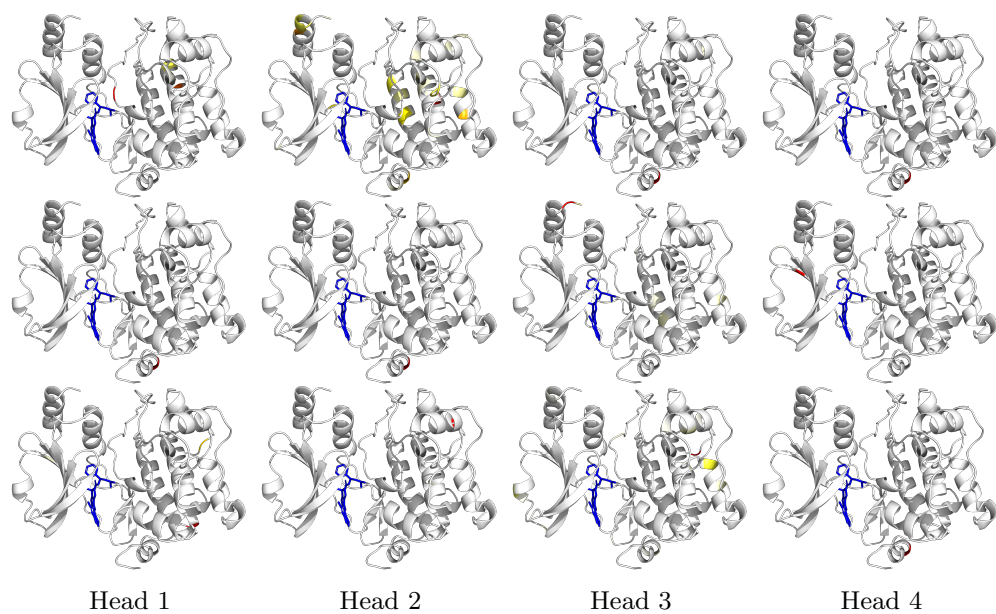


Fig. F5 Analyzing the attention of the ProtBert-1to1 model (trained with 1:1 positive to negative ratio) on PDB ID 2X4Z. Each row is the ProtBert model trained with different seed. Each column is a different attention head. Gradient from white to red indicates the attention weight, where white is no attention and red is max attention for that head. The ligand is shown in blue.

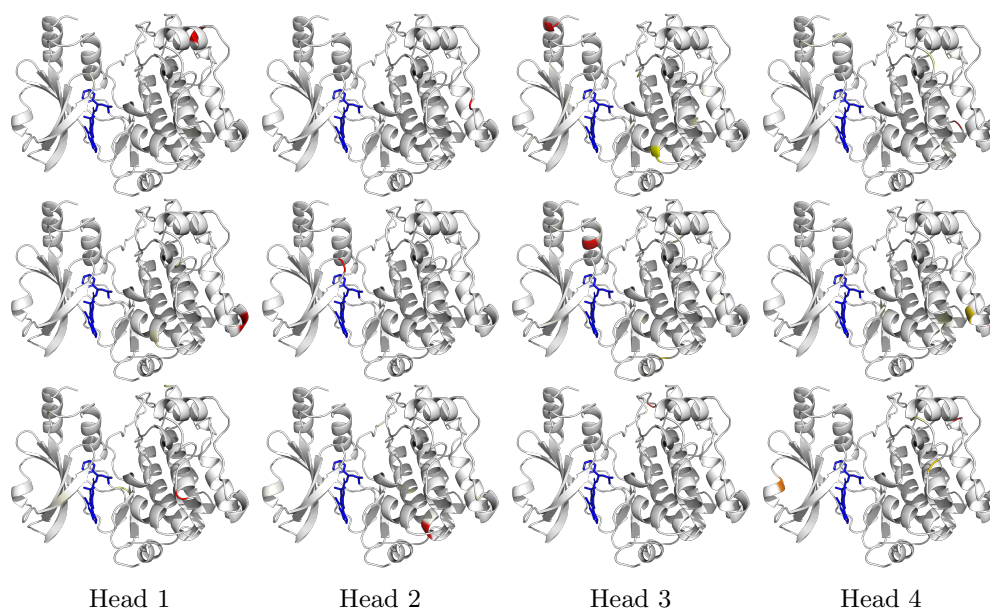


Fig. F6 Analyzing the attention of the SaProt model on PDB ID 2X4Z. Each row is the SaProt model trained with different seed. Each column is a different attention head. Gradient from white to red indicates the attention weight, where white is no attention and red is max attention for that head. The ligand is shown in blue.

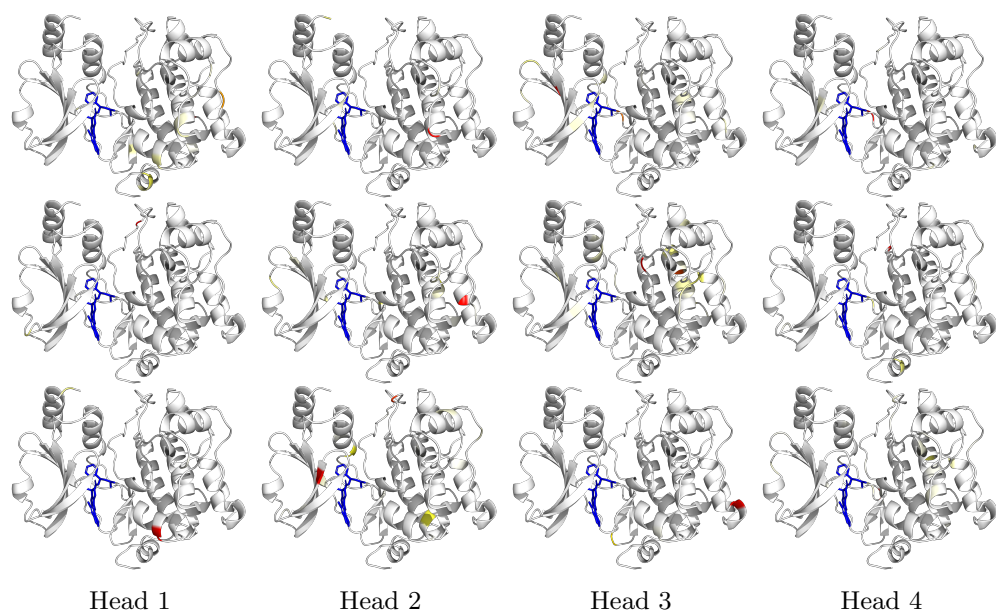


Fig. F7 Analyzing the attention of the SaProt-1to1 model (trained with 1:1 positive to negative ratio) on PDB ID 2X4Z. Each row is the SaProt model trained with different seed. Each column is a different attention head. Gradient from white to red indicates the attention weight, where white is no attention and red is max attention for that head. The ligand is shown in blue.

References

- [1] Sunseri, J. & Koes, D. R. Virtual screening with gina 1.0. *Molecules* **26**, 7369 (2021).
- [2] Singh, R., Sledzieski, S., Bryson, B., Cowen, L. & Berger, B. Contrastive learning in protein language space predicts interactions between drugs and protein targets. *Proceedings of the National Academy of Sciences* **120**, e2220778120 (2023). URL <https://www.pnas.org/doi/10.1073/pnas.2220778120>. Publisher: Proceedings of the National Academy of Sciences.
- [3] World Health Organization. *Antimicrobial resistance: global report on surveillance* (World Health Organization, Geneva, 2014). URL <https://iris.who.int/handle/10665/112642>. Section: xxii, 232 p.
- [4] Colclough, A., Corander, J., Sheppard, S. K., Bayliss, S. C. & Vos, M. Patterns of cross-resistance and collateral sensitivity between clinical antibiotics and natural antimicrobials. *Evolutionary applications* **12**, 878–887 (2019).
- [5] Morgan, H. L. The Generation of a Unique Machine Description for Chemical Structures-A Technique Developed at Chemical Abstracts Service. *Journal of Chemical Documentation* **5**, 107–113 (1965). URL <https://doi.org/10.1021/c160017a018>. Publisher: American Chemical Society.
- [6] Brandes, N., Ofer, D., Peleg, Y., Rappoport, N. & Linial, M. ProteinBERT: a universal deep-learning model of protein sequence and function. *Bioinformatics* **38**, 2102–2110 (2022). URL <https://doi.org/10.1093/bioinformatics/btac020>.
- [7] Rives, A. *et al.* Biological structure and function emerge from scaling unsupervised learning to 250 million protein sequences. *Proceedings of the National Academy of Sciences* **118** (2021). URL <http://dx.doi.org/10.1073/pnas.2016239118>.
- [8] Su, J. *et al.* SaProt: Protein Language Modeling with Structure-aware Vocabulary (2024). URL <https://www.biorxiv.org/content/10.1101/2023.10.01.560349v4>. Pages: 2023.10.01.560349 Section: New Results.
- [9] Gao, B. *et al.* Drugclip: Contrastive protein-molecule representation learning for virtual screening. *Advances in Neural Information Processing Systems* **36** (2024).
- [10] Jia, Y. *et al.* Deep contrastive learning enables genome-wide virtual screening. *bioRxiv* 2024–09 (2024).
- [11] Meller, A. *et al.* Predicting locations of cryptic pockets from single protein structures using the pocketminer graph neural network. *Nature Communications* **14**, 1177 (2023).

- [12] Van Kempen, M. *et al.* Fast and accurate protein structure search with foldseek. *Nature biotechnology* **42**, 243–246 (2024).
- [13] Chroma. Chroma - the open-source embedding database. <https://www.trychroma.com/> (2024).
- [14] Zhang, Z. *et al.* Protein language models learn evolutionary statistics of interacting sequence motifs. *bioRxiv* 2024–01 (2024).
- [15] Touvron, H. *et al.* Augmenting convolutional networks with attention-based aggregation. *arXiv preprint arXiv:2112.13692* (2021).
- [16] Golts, A. *et al.* A large dataset curation and benchmark for drug target interaction. *arXiv preprint arXiv:2401.17174* (2024).
- [17] Kim, S. *et al.* Pubchem 2023 update. *Nucleic acids research* **51**, D1373–D1380 (2023).
- [18] Gilson, M. K. *et al.* Bindingdb in 2015: a public database for medicinal chemistry, computational chemistry and systems pharmacology. *Nucleic acids research* **44**, D1045–D1053 (2016).
- [19] Gaulton, A. *et al.* The chembl database in 2017. *Nucleic acids research* **45**, D945–D954 (2017).
- [20] Spitzer, R. & Jain, A. N. Surflex-dock: Docking benchmarks and real-world application. *Journal of computer-aided molecular design* **26**, 687–699 (2012).
- [21] Halgren, T. A. *et al.* Glide: a new approach for rapid, accurate docking and scoring. 2. enrichment factors in database screening. *Journal of medicinal chemistry* **47**, 1750–1759 (2004).
- [22] Zhang, X. *et al.* Planet: A multi-objective graph neural network model for protein-ligand binding affinity prediction. *bioRxiv* (2023).
- [23] McNutt, A. T. *et al.* Gnina 1.0: molecular docking with deep learning. *Journal of cheminformatics* **13**, 43 (2021).
- [24] Öztürk, H., Özgür, A. & Ozkirimli, E. Deepdta: deep drug–target binding affinity prediction. *Bioinformatics* **34**, i821–i829 (2018).
- [25] Brocchiacono, M. *et al.* Bigbind: learning from nonstructural data for structure-based virtual screening. *Journal of Chemical Information and Modeling* **64**, 2488–2495 (2023).
- [26] Tran-Nguyen, V.-K., Jacquemard, C. & Rognan, D. Lit-pcba: an unbiased data set for machine learning and virtual screening. *Journal of chemical information and modeling* **60**, 4263–4273 (2020).

- [27] Wallach, I. & Heifets, A. Most ligand-based classification benchmarks reward memorization rather than generalization. *Journal of chemical information and modeling* **58**, 916–932 (2018).
- [28] Steinegger, M. & Söding, J. Mmseqs2 enables sensitive protein sequence searching for the analysis of massive data sets. *Nature biotechnology* **35**, 1026–1028 (2017).
- [29] Huang, K. *et al.* Artificial intelligence foundation for therapeutic science. *Nature chemical biology* **18**, 1033–1036 (2022).
- [30] Lam, H. T. *et al.* Otter-knowledge: benchmarks of multimodal knowledge graph representation learning from different sources for drug discovery. *arXiv preprint arXiv:2306.12802* (2023).
- [31] Ackloo, S. *et al.* Cache (critical assessment of computational hit-finding experiments): A public–private partnership benchmarking initiative to enable the development of computational methods for hit-finding. *Nature Reviews Chemistry* **6**, 287–295 (2022).
- [32] Yazdani, S. *et al.* Genetic variability of the sars-cov-2 pocketome. *Journal of Proteome Research* **20**, 4212–4215 (2021).
- [33] Koes, dunn [u. of pittsburgh] computational methods - cache2. URL <https://cache-challenge.org/challenges/app/63160acad0a52>.
- [34] Gentile, F. *et al.* Deep docking: a deep learning platform for augmentation of structure based drug discovery. *ACS central science* **6**, 939–949 (2020).
- [35] Modi, V. & Dunbrack Jr, R. L. A structurally-validated multiple sequence alignment of 497 human protein kinase domains. *Scientific reports* **9**, 19790 (2019).
- [36] Setiya, A., Jani, V., Sonavane, U. & Joshi, R. Moltexpred: small molecule toxicity prediction using machine learning approach. *RSC advances* **14**, 4201–4220 (2024).
- [37] Terlouw, B. R. *et al.* Mibig 3.0: a community-driven effort to annotate experimentally validated biosynthetic gene clusters. *Nucleic acids research* **51**, D603–D610 (2023).
- [38] Landrum, G. *et al.* Rdkit: Open-source cheminformatics. <https://www.rdkit.org> (2024).
- [39] Jumper, J. *et al.* Highly accurate protein structure prediction with alphafold. *nature* **596**, 583–589 (2021).
- [40] Davis, M. I. *et al.* Comprehensive analysis of kinase inhibitor selectivity. *Nature biotechnology* **29**, 1046–1051 (2011).

- [41] Liu, T., Lin, Y., Wen, X., Jorissen, R. N. & Gilson, M. K. Bindingdb: a web-accessible database of experimentally determined protein–ligand binding affinities. *Nucleic acids research* **35**, D198–D201 (2007).
- [42] Zitnik, M., Soscic, R. & Leskovec, J. Biosnap datasets: Stanford biomedical network dataset collection. *Note: <http://snap.stanford.edu/biodata>* Cited by **5** (2018).
- [43] Huang, K., Xiao, C., Glass, L. M. & Sun, J. Moltrans: molecular interaction transformer for drug–target interaction prediction. *Bioinformatics* **37**, 830–836 (2021).
- [44] Li, J. *et al.* Leak proof pddbbind: A reorganized dataset of protein-ligand complexes for more generalizable binding affinity prediction. *arXiv preprint arXiv:2308.09639* (2023).
- [45] Frolova, D. *et al.* Mulan: Multimodal protein language model for sequence and structure encoding. *bioRxiv* 2024–05 (2024).
- [46] Wang, D. *et al.* S-plm: Structure-aware protein language model via contrastive learning between sequence and structure. *bioRxiv* (2024). URL <https://www.biorxiv.org/content/early/2024/01/28/2023.08.06.552203>.
- [47] Zhou, G. *et al.* Uni-mol: A universal 3d molecular representation learning framework (2023).
- [48] Ji, X. *et al.* Uni-mol2: Exploring molecular pretraining model at scale. *arXiv preprint arXiv:2406.14969* (2024).
- [49] Simon, E. & Zou, J. Interplm: Discovering interpretable features in protein language models via sparse autoencoders. *bioRxiv* 2024–11 (2024).
- [50] Atanasov, A. G., Zotchev, S. B., Dirsch, V. M. & Supuran, C. T. Natural products in drug discovery: advances and opportunities. *Nature reviews Drug discovery* **20**, 200–216 (2021).
- [51] Kishimoto, A. *et al.* MHG-GNN: Combination of Molecular Hypergraph Grammar with Graph Neural Network (2023). URL <http://arxiv.org/abs/2309.16374>. ArXiv:2309.16374 [cs].
- [52] Ross, J. *et al.* Large-Scale Chemical Language Representations Capture Molecular Structure and Properties (2022). URL <http://arxiv.org/abs/2106.09553>. ArXiv:2106.09553 [cs, q-bio].
- [53] Stokes, J. M. *et al.* A deep learning approach to antibiotic discovery. *Cell* **180**, 688–702 (2020).

- [54] Mongia, M., Guler, M. & Mohimani, H. An interpretable machine learning approach to identify mechanism of action of antibiotics. *Scientific Reports* **12**, 10342 (2022).
- [55] Cremer, J., Medrano Sandonas, L., Tkatchenko, A., Clevert, D.-A. & De Fabritiis, G. Equivariant graph neural networks for toxicity prediction. *Chemical Research in Toxicology* **36**, 1561–1573 (2023).
- [56] Mirdita, M. *et al.* Colabfold: making protein folding accessible to all. *Nature methods* **19**, 679–682 (2022).
- [57] Liu, Z. *et al.* Forging the basis for developing protein–ligand interaction scoring functions. *Accounts of chemical research* **50**, 302–309 (2017).
- [58] Gazizov, A., Lian, A., Goverde, C. A., Ovchinnikov, S. & Polizzi, N. F. Af2bind: Predicting ligand-binding sites using the pair representation of alphafold2. *bioRxiv* 2023–10 (2023).